SolarPACES 2022, 28th International Conference on Concentrating Solar Power and Chemical Energy Systems
Advanced Materials, Manufacturing, and Components
https://doi.org/10.52825/solarpaces.v1i.680

Published: 21 Mar. 2024

Heat Transfer of an Integrated Counterflow Ceramic Heat Exchanger

Wenhua Yu[1][https://orcid.org/0000-0002-1945-7014], David M. France[1][https://orcid.org/0009-0008-0039-9791], Robert A. Erck[1][https://orcid.org/0000-0002-0356-3920], and Dileep Singh[1]

[1] Argonne National Laboratory, USA

Abstract. The ceramic-based heat exchanger is one of the leading contenders for high-efficiency concentrating solar power plants using a molten salt heat transfer fluid and a supercritical carbon dioxide Brayton power cycle operating at temperatures above 700 °C due to the excellent resistance of ceramics to corrosion, oxidation, erosion, creep, and fouling. In the present study, the thermal performance of a ceramic silicon carbide prototype heat exchanger, with semi-elliptical heat transfer channels, integrated header channels, and a counterflow configuration fabricated by using binder jetting additive manufacturing, was experimentally investigated. Experimental heat transfer tests of the prototype were conducted at high temperatures and under various test fluid flow rates and inlet temperatures. The experimental heat transfer rates compared favorably with simulation predictions.

Keywords: Ceramic, Heat Exchanger, Heat Transfer, Concentrating Solar Power

1. Introduction

The supercritical carbon dioxide (CO_2) Brayton power cycle is being considered as a highly-efficient power generation cycle to be integrated with solar receivers for the next-generation concentrating solar power plants [1]. In one of such supercritical CO_2 systems, molten salts are used as heat transfer fluids for transferring heat from solar receivers to the supercritical CO_2 working fluid at temperatures above 700 °C [2]. These application conditions present multiple challenges for one of the essential components, the heat exchanger. Metal alloy-based heat exchangers will not survive under such high operating pressures and temperatures and corrosive environments due to corrosion, oxidation, erosion, creep, and fouling. Ceramic-based HXs have been investigated for such extreme application conditions [3]. In our previous work, a ceramic silicon carbide-based heat exchanger with flow channels of a semi-elliptic cross section was developed [4], and its heat transfer performance was measured through experiments on a lab-scale prototype at relatively low temperatures [5]. In the present study, the heat transfer performance of this test prototype was further investigated at high temperatures and under various test fluid flow rates and inlet temperatures. The results from the present study further extend our previous low-temperature testing ones [5] and contribute towards the targeted application conditions of temperatures above 700 °C.

2. Design and fabrication of lab-scale prototype heat exchanger

The lab-scale prototype was designed in Fusion 360 by taking into consideration the stresses that would be experienced by a full-size ceramic heat exchanger. The full-size heat exchanger was optimized for coupled heat transfer and stress through an iterative process under the operation conditions of (a) a molten salt as the heat transfer fluid with an inlet temperature of

750 °C and an outlet temperature of 570 °C, (b) supercritical CO_2 as the working fluid with an inlet temperature of 540 °C and an outlet temperature of 700 °C, and (c) a supercritical CO_2 operation pressure of 20 MPa. The optimized full-size heat exchanger had a semi-ellipse (a modified ellipse with a rectangular section in the middle) flow channel cross section [4]. The lab-scale prototype is of a similar semi-elliptical flow channel cross section. It contains eight layers of channels with four channels in each layer yielding a total of 16 channels for the first heat transfer fluid and another 16 channels for the second heat transfer fluid as shown in the simulation results of Figure 7. The lab-scale prototype also contains integrated header channels connected to protruding inlet and outlet ports [5].

The lab-scale prototype was fabricated in several steps. First, the lab-scale prototype was additively manufactured from SiC powder by using binder jetting printing. For this step, the printer (Innovent+, ExOne Inc., USA) feedstock was alpha-phase silicon carbide powder with an average particle size of 50 μm and irregular shape (SCG 240HD, Panadyne Inc., USA). The printer used an STL design file obtained from Fusion 360. Printing parameters for the lab-scale prototype were optimized through test printings. The printed and debound lab-scale prototype was not fully dense. To close internal pores, several liquid polymer infiltration and pyrolysis process steps were then performed. The measured weight increased rapidly for the first four liquid polymer infiltration and pyrolysis cycles, showing that the pores were being filled. Additional cycles were performed to completely close the internal pore connections among the fluid channels [5].

3. Experimental test facility

Heat transfer experiments were conducted in an test facility consisting of two independently controllable cold and hot air flow loops. As shown in Figure 1, each flow loop contained an air pump, a flow controller, a flowmeter, a controllable air heater, and thermocouples at the inlets and outlets of the test prototype. In both the cold and hot air flow loops, air was pumped by the air pumps through the flow controllers, flowmeters, and controllable air heaters, entering the inlets of the test prototype at desired cold and hot air inlet temperatures. The two air flows were in a counterflow configuration. During experimental tests, the test prototype was placed in a furnace.

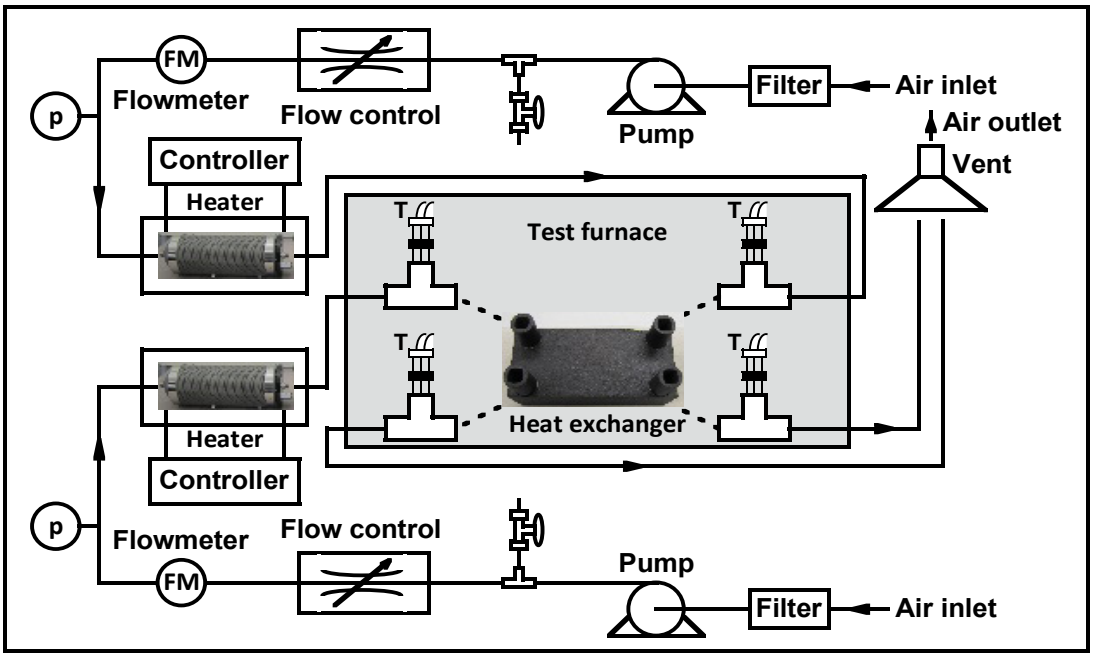

Figure 1. Experimental test facility.

4. Experimental tests and results

4.1 Heat gain and loss calibration

The test prototype was well insulated thermally and was placed in the furnace maintained at a constant temperature during experimental tests to minimize the heat gain from or heat loss to the environment. However, the heat gain or loss was not eliminated completely due to the small flow channels, low air flow rates, and relatively high driving temperatures. The heat gain or loss was measured experimentally, and results were incorporated into experimental data reduction for improving accuracy.

The heat gain and loss were calibrated through specially designed experiments. For the heat gain calibrations, air flowed through only the cold air channels of the test prototype, and the furnace was heated. Because there was no air flowing through the hot air channels of the test prototype, the temperature rise in the cold air from the inlet to the outlet was caused by the heat gained from the hotter furnace air. This heat gain can be characterized by the following equation

$$\dot{m}_{cold\ air} c_p (T_{cold\ air\ outlet} - T_{cold\ air\ inlet}) = c_{heat\ gain} \Delta T_{furnace\text{-}cold\ air} \quad (1)$$

where $\dot{m}$ is the mass flow rate, c_p is the mass specific heat capacity, T is the temperature, $c_{heat\ gain}$ is a constant determined from the heat gain tests, and the heat gain driving temperature is defined as the temperature difference between the furnace and the average of the cold air inlet and outlet. For the heat loss calibrations, air flowed through only the hot air channels of the test prototype, and the furnace was not heated but its temperature rose due to the heat from the hotter air flow. Because there was no air flowing through the cold air channels of the test prototype, the temperature decrease in the hot air from the inlet to the outlet was caused by the heat lost to the colder furnace air. This heat loss can be characterized by the following equation

$$\dot{m}_{hot\ air} c_p (T_{hot\ air\ inlet} - T_{hot\ air\ outlet}) = c_{heat\ loss} \Delta T_{hot\ air\text{-}furnace} \quad (2)$$

Where $c_{heat\ loss}$ is a proportional constant determined from the heat loss tests and the heat loss driving temperature is defined as the temperature difference between the average of the hot air inlet and outlet and the furnace. The heat gain and loss calibration results are shown in Figure 2. The linear plots of Figure 2 are typical of these types of heat gains and losses.

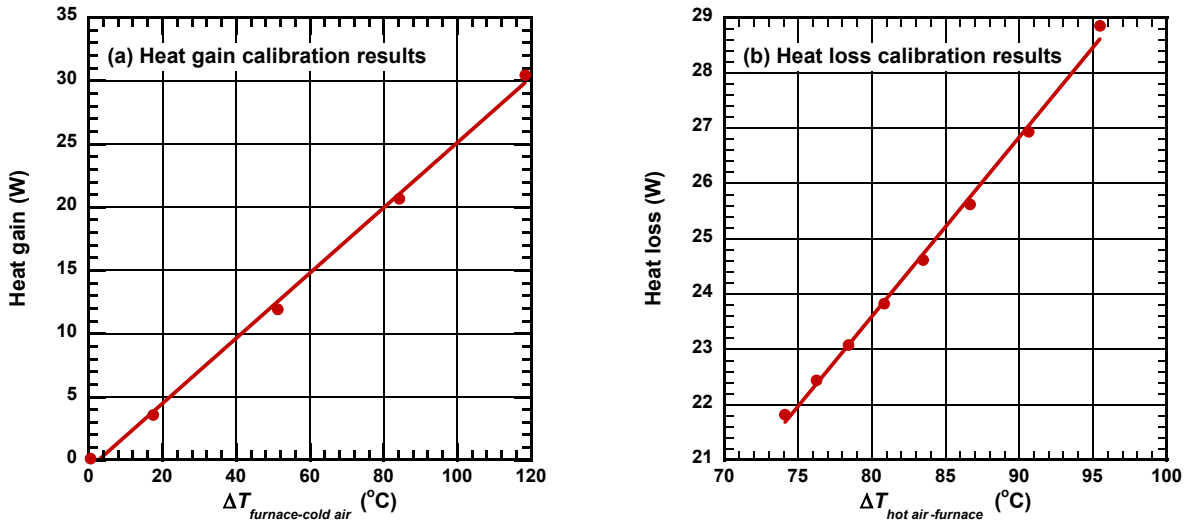

Figure 2. Heat gain and loss calibration results.

4.2 Flow rate effects on the heat transfer rate

In the present study, heat transfer experiments were conducted for three cold air flow rates of 87.5 SCFH, 112.5 SCFH, and 129 SCFH and three hot air flow rates of 140 SCFH, 150 SCFH, and 160 SCFH, where one standard cubic foot per hour (SCFH) is 0.00787 l/s. The hot air temperature at the inlet of the test prototype was adjusted to 540–560 °C, and the inlet temperature difference between the hot and cold air flows was adjusted to approximately 200 °C. During experiments, the flow rates, inlet temperatures, and outlet temperatures of both the cold and hot air flows were displayed on-screen of a data acquisition system for monitoring testing status. Fifty readings of the sensor outputs were recorded when a steady-state condition was reached.

Based on the experimental data, the heat transfer rate was calculated for both the cold and hot air flows. The heat balance between the heat transfer rates of the cold and hot air flows was checked for each experimental test. The relative heat transfer difference, $r_{\dot{q}_{hot\ air\ vs\ cold\ air}}$, was calculated by the following equation

$$r_{\dot{q}_{hot\ air\ vs\ cold\ air}} = (\dot{q}_{hot\ air} - \dot{q}_{cold\ air}) / [(\dot{q}_{hot\ air} + \dot{q}_{cold\ air})/2] \quad (3)$$

where $\dot{q}$ is the heat transfer rate. The maximum relative heat transfer rate difference is 6.54%. These results served as verification of the overall experimental results, including experimental measurements, heat gain and loss calibrations, and experimental data reduction procedures.

Figure 3 shows the flow rate effects on the heat transfer rate calculated as an average heat transfer rate of the cold and hot air flows. As shown in Figure 3, the heat transfer rate increases with both the cold and hot air flow rates as expected. This trend is similar to that from the lower-temperature experiments [5]. It is expected that the heat transfer rate will continue to increase with increased cold and hot air flow rates beyond those tested.

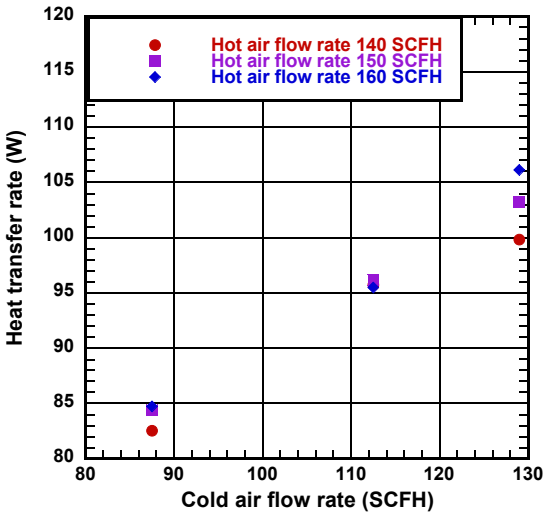

Figure 3. Flow rate effects on the heat transfer rate.

As further verification, two additional sets of repeating tests were conducted for two hot air flow rates of 140 SCFH and 150 SCFH. The flow rates and inlet temperatures of the cold and hot air flows were kept similar to those of the first set of experimental tests with an inlet temperature difference of approximately 200 °C between the hot and cold air flows. The heat transfer rate as functions of the air flow rate is shown in Figure 4. As shown in Figure 4, the heat transfer rates for all three test sets follow a similar trend with the maximum relative difference of 3.69% between them. The deviation is within the experimental uncertainty and might be caused by slight differences of the air inlet temperatures.

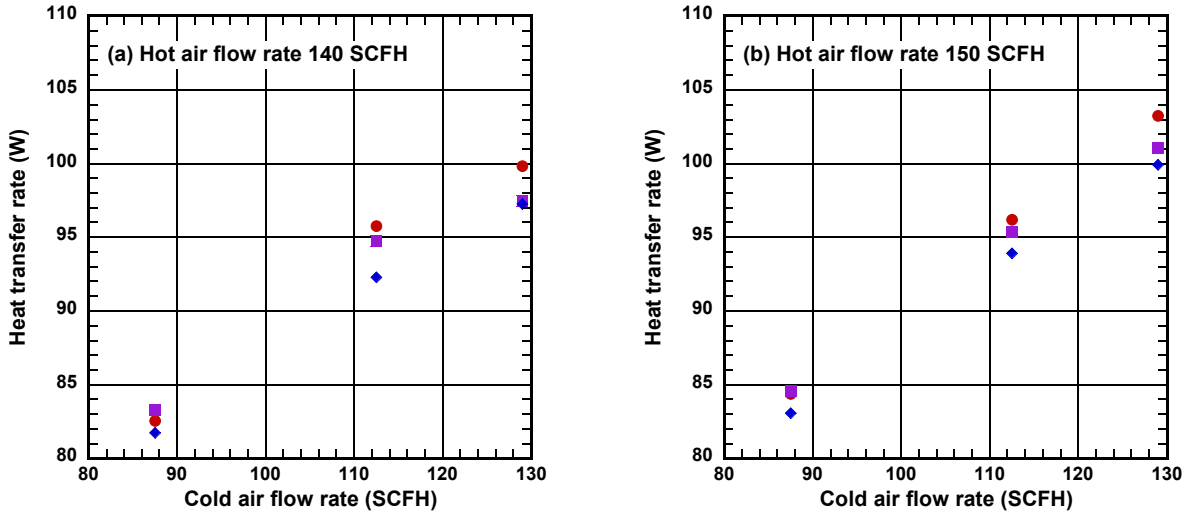

Figure 4. Experimental repeatability (different symbols indicating different test sets).

4.3 Inlet temperature difference effects on the heat transfer rate

To investigate the effects of the inlet temperature difference between the hot and cold air flows, $\Delta T_{inlet}=T_{hot\ air\ inlet}-T_{cold\ air\ inlet}$, on the heat transfer rate, experimental tests were conducted for two additional inlet temperature differences of approximately 160 °C and 240 °C. The tests were conducted for three cold air flow rates of 87.5 SCFH, 112.5 SCFH, and 129 SCFH and two hot air flow rates of 140 SCFH and 150 SCFH. Figure 5 illustrates the effects of the inlet temperature difference on the heat transfer rate. As shown in Figure 5, the heat transfer rates for three inlet temperature differences follow very similar heat transfer increase trends to the cold and hot air flow rate trends. The heat transfer rates increase with the inlet temperature difference as expected. The flow rate and temperature difference effects, on heat exchanger heat transfer rates, show the additively manufactured prototype to be functioning normally without structural problems.

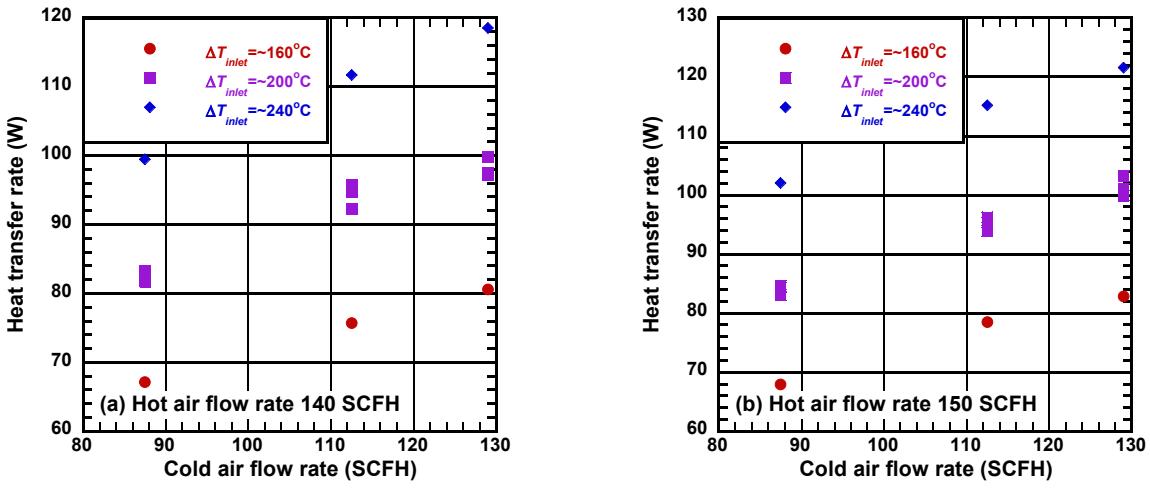

Figure 5. Inlet temperature difference effects on the heat transfer rate.

4.4 Thermal cycle effects on the heat transfer rate

High-temperature exposure and thermal cycle effects on the heat transfer were also investigated through the following processes. First, the test prototype was heated to approximately 700 °C and kept at that temperature for one hour by using the controlled furnace heating. Then,

the furnace heating control program was stopped, and the test prototype was cooled to room temperature. After one thermal cycle, heat transfer experiments were conducted for three cold air flow rates of 87.5 SCFH, 112.5 SCFH, and 129 SCFH and two hot air flow rates of 140 SCFH and 150 SCFH. The inlet temperatures of the hot and cold air flows were adjusted to be similar to those for pre-thermal cycling with an inlet temperature difference between the hot and cold air flows of approximately 200 °C. Additionally, five of the same thermal cycles were conducted on the test prototype. Heat transfer experiments were conducted under similar testing conditions. As shown in Figure 6, the heat transfer rates for the post-thermal cycle experiments agree well with those for the pre-thermal cycling with a maximum relative difference of 4.88% between them.

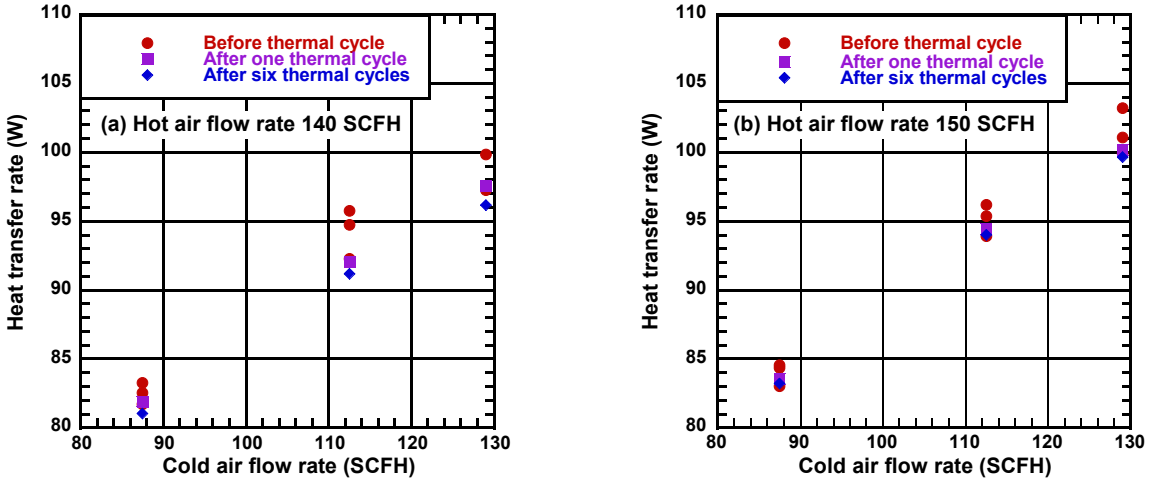

Figure 6. Thermal cycle effects on the heat transfer rate.

4.5 Comparison of experimental data and simulated results

To verify the viability of simulation models for the design of the ceramic heat exchanger and for the prediction of its thermal performance, the experimental data were compared with simulated results. In the present study, numerical simulations for the test prototype were conducted by using the COMSOL Multiphysics commercial software. The three-dimensional computation model simulated the test prototype geometry under uniform flow distribution through all flow channels without the effects of the header channels. For each experimental test, the measured flow rates and inlet temperatures of the cold and hot air flows were used as simulation inputs, and the outlet temperatures of the cold and hot air flows were computed as model outputs. As an example, Figure 7 illustrates the simulated temperature distribution for one of the experimental tests with a cold air flow rate of 112.5 SCFH, a hot air flow rate of 150 SCFH, a cold air inlet temperature of 355 °C, and a hot air inlet temperature of 557 °C. Based on the experimental parameters, the prototype heat transfer rates were calculated and compared with the experimental data for all cold and hot air flow rates. The relative heat transfer difference, $r_{\dot{q}_{experimental\ vs\ simulated}}$, between the experimental data and the simulated values, was calculated for each experimental test by the following equation

$$r_{\dot{q}_{experimental\ vs\ simulated}} = \left(\dot{q}_{experimental} - \dot{q}_{simulated}\right) / \left[\left(\dot{q}_{experimental} + \dot{q}_{simulated}\right)/2\right] \quad (4)$$

The results show that the maximum relative heat transfer difference is less than 15%, which is considered reasonable. The potential causes for the differences include the test prototype header effect that was not considered in the simulation model and the heat gain and loss effect that was not modelled perfectly in the simulations. Also, any flow maldistribution among channels was not included in the simulations.

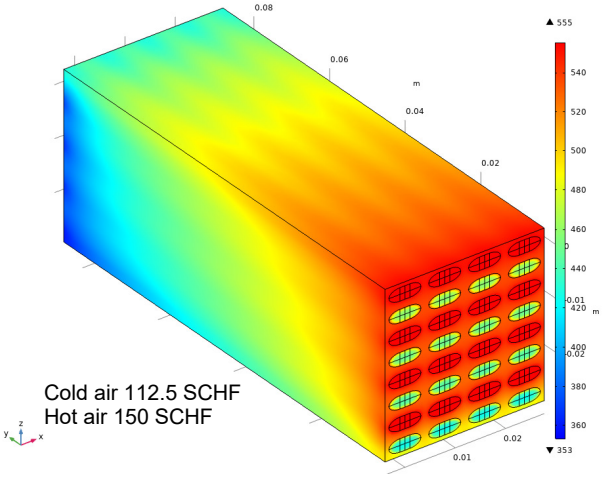

Figure 7. Simulated temperature distribution.

5. Conclusions

Heat transfer of a ceramic prototype heat exchanger was experimentally investigated at elevated temperatures with the hot air inlet temperature in the range of 540–560 °C. The following are the key results and conclusions.

The maximum relative heat transfer rate difference was 6.54% between the hot and cold air flows in the experiments. These results served as verification of the overall experimental results, including experimental measurements, heat gain and loss calibrations, and experimental data reduction procedures.

Average heat transfer rates were calculated for three cold air flow rates and three hot air flow rates. The heat transfer rate increases with both the cold and hot air flow rates. This trend is similar to that from the lower-temperature experiments. It is expected that the heat transfer rate will continue to increase with increased cold and hot air flow rates beyond those tested.

The effects of the inlet temperature difference between the hot and cold air flows were investigated. The result show that the heat transfer rates for three inlet temperature differences follow very similar increase trends to the cold and hot air flow rate trends. The heat transfer rates increase with the inlet temperature difference. The flow rate and temperature difference effects, on heat exchanger heat transfer rates, show the additively manufactured prototype to function normally without structural problems.

Heat transfer experiments were conducted to the test prototype after one and six thermal cycles at 700 °C. The results show that the heat transfer rates for the post-thermal cycle experiments agree well with those for pre-thermal cycling.

Numerical simulations were conducted based on the experimental conditions by assuming a uniform flow distribution in the flow channels. The results show that the maximum relative heat transfer difference between the experimental data and the simulated values is less than 15%, which is considered reasonable. The prediction accuracy can be further improved by including test prototype header and flow distribution effects.

Overall, the results of this study show the integrity of the additively manufactured ceramic heat exchanger at temperatures up to 700 °C. The results form the basis for further development, of a full-size ceramic heat exchanger using the additive manufacturing approach, with significant cost savings over conventional manufacturing methods.

Data availability statement

Data will be made available on request.

Author contributions

W. Yu–Conceptualization, methodology, validation, formal analysis, investigation, and writing (original draft). D. M. France–Conceptualization, methodology, formal analysis, and writing (review & editing). R. A. Erck–Methodology, resources, and writing (review & editing). D. Singh–Conceptualization, methodology, resources, writing (review & editing), supervision, project administration, and funding acquisition.

Competing interests

The authors declare that they have no competing interests.

Funding

This material is based upon work supported by the U.S. Department of Energy's Office of Energy Efficiency and Renewable Energy (EERE) under the Solar Energy Technologies Office (SETO) Award Number 34240 at Argonne National Laboratory operated under Contract no. DE-AC02-06CH11357 by the UChicago Argonne, LLC.

Acknowledgement

Fruitful discussions with Drs. Kamala Raghavan and Vijaykumar Rajgopal, SETO program managers, are much appreciated. The authors thank Dr. Wenchao Du for his help on the test prototype fabrication and Dr. I-Han Liu for her help on the numerical simulation.

References

1. M. Mehos, C. Turchi, J. Vidal, M. Wagner, Z. Ma, C. Ho, W. Kolb, C. Andraka, A. Kruizenga, "Concentrating Solar Power Gen3 Demonstration Roadmap," National Renewable Energy Laboratory, Golden CO, USA, 2017.
2. Y. Ahn, S. J. Bae, M. Kim, S. K. Cho, S. Baik, J. I. Lee, J. E. Cha, "Review of Supercritical CO_2 Power Cycle Technology and Current Status of Research and Development," Nucl. Eng. Technol., vol.47, pp. 647–661, 2015, doi: https://doi.org/10.1016/j.net.2015.06.009.
3. J. Schulte-Fischedick, V. Dreißigacker, R. Tamme, "An Innovative Ceramic High Temperature Plate-Fin Heat Exchanger for EFCC Processes," Appl. Therm. Eng., vol.27, 1285–1294, 2007, https://doi.org/10.1016/J.APPLTHERMALENG.2006.11.007.
4. D. Singh, W. Yu, D. M. France, T. P. Allred, I.-H. Liu, W. Du, B. Barua, M. C. Messner, "One Piece Ceramic Heat Exchanger for Concentrating Solar Power Electric Plants," Renew. Energy, vol.160, pp. 1308–1315, 2020, doi: https://doi.org/10.1016/j.renene.2020.07.070.
5. W. Du, W. Yu, D. M. France, M. Singh, D. Singh, "Additively Manufacturing and Testing of a Ceramic Heat Exchanger for High-Temperature and High-Pressure Applications for Concentrating Solar Power," Sol. Energy, vol.236, pp. 654–665, 2022, doi: https://doi.org/10.1016/j.solener.2022.03.046.